Latent Pose Estimator for Continuous Action Recognition

Huazhong Ning[1], Wei Xu[2], Yihong Gong[2], and Thomas Huang[1]

[1] ECE, U. of Illinois at Urbana-Champaign, USA
{hning2,huang}@ifp.uiuc.edu
[2] NEC Laboratories America, Inc., USA
{xw,ygong}@sv.nec-labs.com

Abstract. Recently, models based on conditional random fields (CRF) have produced promising results on labeling sequential data in several scientific fields. However, in the vision task of continuous action recognition, the observations of visual features have dimensions as high as hundreds or even thousands. This might pose severe difficulties on parameter estimation and even degrade the performance. To bridge the gap between the high dimensional observations and the random fields, we propose a novel model that replace the observation layer of a traditional random fields model with a latent pose estimator. In training stage, the human pose is not observed in the action data, and the latent pose estimator is learned under the supervision of the labeled action data, instead of image-to-pose data. The advantage of this model is twofold. First, it learns to convert the high dimensional observations into more compact and informative representations. Second, it enables transfer learning to fully utilize the existing knowledge and data on image-to-pose relationship. The parameters of the latent pose estimator and the random fields are jointly optimized through a gradient ascent algorithm. Our approach is tested on HumanEva [1] – a publicly available dataset. The experiments show that our approach can improve recognition accuracy over standard CRF model and its variations. The performance can be further significantly improved by using additional image-to-pose data for training. Our experiments also show that the model trained on HumanEva can generalize to different environment and human subjects.

1 Introduction

Recognizing human actions in videos with natural environments provides an infrastructure for a wide range of applications spanning visual surveillance, systems for entertainment, human-computer interfaces, and so on. It is a specific example of a widely studied problem of sequence labeling that arises in several scientific fields. A well understood and widely used probabilistic model for this problem is Hidden Markov Model (HMM) [2]. But HMMs make strict assumption that observations are conditionally independent given class labels, and cannot represent multiple interacting features and long-range dependencies of the observations. Thus, it largely limits the applicability of the HMM models.

D. Forsyth, P. Torr, and A. Zisserman (Eds.): ECCV 2008, Part II, LNCS 5303, pp. 419–433, 2008.

Conditional random fields models [3] relax the assumption of observation independency and has exhibited success to discriminate actions in both segmented and unsegmented video sequences [4,5]. In [4], a latent-dynamic conditional random field (LDCRF) model is proposed to capture both extrinsic dynamics and intrinsic structure of head and gaze aversion gestures. The poses of 3D head or eye gaze are robustly estimated using a view based appearance model, and the model recognizes the gestures based on the pose representations. However, in action recognition where articulated human body is involved, the explicit pose of the body parts could not be reliably estimated by currently existing tracking algorithms. In other words, it is impractical to use LDCRF to recognize complex human actions in the same way as in [4]. An possible solution is to directly feed the visual features (*e.g.*, block SIFT [6] and silhouette[7]), instead of human poses, to the random fields as in [5] where a chain conditional random fields (CRF) model [3] is used. But the dimension of visual features is usually as high as hundreds or even thousands, compared to 10-50 dimensions of human poses, and their discriminative power to represent human actions is also worse than human poses. This might increase the complexity of parameter estimation in random fields while degrade the performance.

In this paper, we propose a novel model to bridge the gap between the high dimensional visual features and the random fields. As we know, human pose is a very compact and informative representation for human images. And recently, the multi-modal image-to-pose relationship has been successfully exploited using discriminative models, such as linear/nonlinear regression [7], Bayesian mixture of experts (BME) [6], and so on. Therefore, we propose a model that replaces the observation layer of the random fields with an image-to-pose discriminative model. Fig. 1 illustrates the graphical structure of our model. This image-to-pose layer learns to convert the high dimensional observations into more compact and informative representations (such as poses of articulated human body) under the supervision of labeled action data. We call it *latent pose estimator*, because it is not explicitly estimated from labeled image-to-pose data. Actually, the human poses are not observed in action training data. Of course, additional image-to-pose data, if available, can also be added to the learning process. In practice, the output of the latent pose estimator can be human pose (image-to-pose data are enough) or any other compressed representations (not enough or no pose data), but we still use the term “pose estimator”. We call our model *latent pose conditional random fields (LPCRF)*. In this paper, our model is based on LDCRF, but it can be extended to any other CRF variations. Our experiments show that the use of latent pose estimator can improve recognition accuracy over traditional CRF or LDCRF even without using any image-to-pose data for training.

The structure of our LPCRF model not only maintains the strength of the LDCRF model in that it captures both extrinsic dynamics and internal substructure, but also enables the model to recognize actions from high dimensional visual features without increasing the complexity of the feature functions. Due

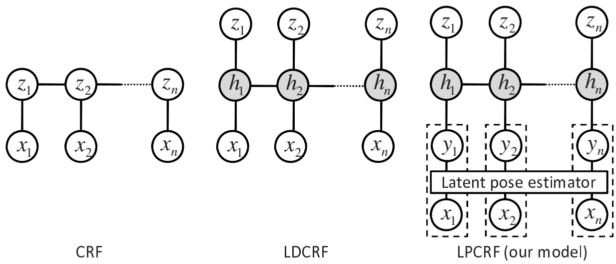

Fig. 1. Graphical structures of our LPCRF model and two existing models: CRF [3] and LDCRF [4]. In these models, $\mathbf{x}$ is a visual observation, z is the class label (*e.g.*, walking or hand waving) assigned to $\mathbf{x}$, and h represents a hidden state of human actions (*e.g.*, left-to-right/right-to-left walking). The subscripts index the frame number of the video sequence. In our LPCRF model, the observation layer of the random fields is replaced with a *latent pose estimator* that learns to compress the high dimensional visual features $\mathbf{x}$ into a compact representation (like human pose) $\mathbf{y}$. Our model also enables transfer learning to utilize the existing knowledge and data on image-to-pose relationship. The dashed rectangles means that $\mathbf{y}$'s are technically deterministic functions of $\mathbf{x}$ when the parameters of the latent pose estimator are fixed.

to this advantage, our model can recognize human actions with complex articulations in both segmented and unsegmented video sequences.

Another advantage of our LPCRF model is that it enables transfer learning [8] to fully utilize the existing knowledge and data on image-to-pose relationship. Firstly, our model can be incrementally built on an existing discriminative pose estimator that is well-trained on either synthetic or real image-to-pose datasets. More specifically, we use the parameters of an existing pose estimator (if available) to initialize the latent pose estimator. This allows a growing algorithm to acquire new knowledge while keeping old knowledge and to reduce the redevelopment and learning costs. Secondly, newly available image-to-pose data, if available, can be naturally added to the learning process to refine the model parameters without modifying the structure of our model.

The literature that is closely related to our research includes action recognition based on either 2D/3D silhouettes [9,10], 2D body configurations [11], motion trajectories [12], or body kinematics [13]. These works rely on representations of explicit pose or compact silhouette to recognize actions. These representations are generated by a fixed component which cannot be adapted to the given task of action recognition. While in our system, the latent pose estimator is treated as a trainable feature extractor that can be improved with more action data. The benefit of adaptation is clearly demonstrated in our experiments.

2 Latent-Dynamic Conditional Random Fields

First, we briefly introduce the LDCRF model[4] that was proposed to solve the problem of labeling unsegmented video sequences. It incorporates hidden state variables into the traditional CRF [3] to model the sub-structure of human actions, and combines the strengths of CRFs and HCRFs [14] to capture both extrinsic dynamics and intrinsic structure.

Given a sequence of observations $X = \{\mathbf{x}_1, \mathbf{x}_2, \cdots, \mathbf{x}_n\}$, the LDCRF model predicts a sequence of class labels $\mathbf{z} = \{z_1, z_2, \cdots, z_n\}$. Each $\mathbf{x}_i$ is a visual representation for i-th frame. Each $z_i \in \mathcal{Z}$ is the class label of frame $\mathbf{x}_i$, where $\mathcal{Z}$ is the set of all possible class labels of the concerned actions. To model the sub-structure of the actions (*e.g.*, left-to-right/right-to-left walking), a sequence of hidden variables $\mathbf{h} = \{h_1, h_2, \cdots, h_n\}$ is incorporated into the CRF model. Fig. 1 illustrates the graphical structure of the $\mathbf{h}$ layer in LDCRF. These hidden variables are not observed in the training examples, but are instantiated in the predicting stage. The transitions among them model both the substructure patterns of individual actions and the external dynamics between actions.

The LDCRF is restricted to have disjoint sets of hidden states associated with each class label. Denote $\mathcal{H}_z$ the set of hidden states for class z, and $\mathcal{H}_{\mathbf{z}} = \{\mathbf{h} | h_j \in \mathcal{H}_{z_j}, j = 1 \cdots n\}$ the set consisting of all the possible sequences of hidden states compatible with the label sequence $\mathbf{z}$. Let $\mathcal{H} = \sum_{\mathbf{z}} \mathcal{H}_{\mathbf{z}}$ all the possible hidden state sequences. With these definitions, the LDCRF model is defined as

$$P(\mathbf{z}|X, \Phi) = \sum_{\mathbf{h}} P(\mathbf{z}|\mathbf{h}, X, \Phi) P(\mathbf{h}|X, \Phi) = \sum_{\mathbf{h} \in \mathcal{H}_{\mathbf{z}}} P(\mathbf{h}|X, \Phi) \tag{1}$$

where Φ is set of parameters of the model. The second equation is due to the fact that, by definition, $P(\mathbf{z}|\mathbf{h}, X, \Phi) = 1$ for any $\mathbf{h} \in \mathcal{H}_{\mathbf{z}}$, otherwise 0.

Assume the graph for a video sequence is a simple chain. According to the fundamental theorem of random fields [15], the joint distribution over the hidden state sequence $\mathbf{h}$ given X has an exponential form

$$P(\mathbf{h}|X, \Phi) = \frac{1}{K_\Phi(X, \mathcal{H})} \exp\left(\sum_j V_\Phi(j, h_j, X) + \sum_j E_\Phi(j, h_{j-1}, h_j, X) \right), \tag{2}$$

where $K_\Phi(X, \mathcal{H})$ is the observation dependent normalization,

$$K_\Phi(X, \mathcal{H}) = \sum_{\mathbf{h} \in \mathcal{H}} \exp\left(\sum_j V_\Phi(j, h_j, X) + \sum_j E_\Phi(j, h_{j-1}, h_j, X) \right), \tag{3}$$

summarizing over all hidden state sequences in $\mathcal{H}$. And $\Phi = \{\lambda_1, \lambda_2, \cdots, \mu_1, \mu_2, \cdots\}$ is the set of model parameters. $V_\Phi(j, h_j, X)$ and $E_\Phi(j, h_{j-1}, h_j, X)$ are sum of feature functions on individual vertex j and edge $(j-1, j)$, respectively,

$$V_\Phi(j, h_j, X) = \sum_k \lambda_k s_k(j, h_j, X), \tag{4}$$

$$E_\Phi(j, h_{j-1}, h_j, X) = \sum_k \mu_k t_k(j, h_{j-1}, h_j, X). \tag{5}$$

where s_k and t_k are feature functions. s_k are state functions that depend on a single hidden variable of a sub-action in the model, and t_k are transition functions that depend on pairs of hidden variables. We also use V_{ja} and E_{jab} as short representations of $V_\Phi(j, a, X)$ and $E_\Phi(j, a, b, X)$.

3 Latent Pose Conditional Random Fields

Our latent pose conditional random fields (LPCRF) model is a generalization of CRF and LDCRF. Fig. 1 illustrates its graphical structure. The latent pose estimator learns to convert an observation vector $\mathbf{x}$ into a more compact and informative representation $\mathbf{y}$, and the model recognizes human actions based on the pose sequence $Y = \{\mathbf{y}_1, \mathbf{y}_2, \cdots, \mathbf{y}_n\}$. Later we denote the latent pose estimator as $P(\mathbf{y}|\mathbf{x}, \Theta)$ in probabilistic form or $\mathbf{y} = \Psi(\mathbf{x}, \Theta)$ in deterministic form, where Θ is the set of parameters of the latent pose estimator and is jointly optimized with the random fields using a gradient ascent algorithm.

3.1 Formulation of our LPCRF Model

Using the notations and definitions for the LDCRF model in Section 2, our model is defined as

$$P(\mathbf{z}|X, \Omega) = P(\mathbf{z}|Y, \Phi) = \sum_{\mathbf{h} \in \mathcal{H}_\mathbf{z}} P(\mathbf{h}|Y, \Phi) \tag{6}$$

where $Y = \Psi(X, \Theta)$ is the optimal estimation of the latent pose estimator given observations X and parameters Θ, and $\Omega = \{\Phi, \Theta\}$ represents all the model parameters. The joint distribution over the hidden state sequence $\mathbf{h}$ given Y still has an exponential form

$$P(\mathbf{h}|Y, \Phi) = \frac{1}{K_\Phi(Y, \mathcal{H})} \exp\left(\sum_j V_\Phi(j, h_j, Y) + \sum_j E_\Phi(j, h_{j-1}, h_j, Y) \right), \tag{7}$$

where $K_\Phi(Y, \mathcal{H})$ is the observation dependent normalization in Eqn. 3.

If the parameters Θ for the latent pose estimator are fixed, our LPCRF model collapses into an LDCRF model. If each class label $z \in \mathcal{Z}$ is constrained to have only one hidden sub-action, *i.e.*, $|\mathcal{H}_z| = 1$, the LDCRF model further collapses into a CRF model. Hence, our LPCRF model is a more general framework of CRF and LDCRF. However, our LPCRF model is essentially different from both CRF and LDCRF in some aspects. In our model, input features used by the random fields are trainable and are jointly optimized with the random fields, while in CRF and LDCRF, the input features are fixed and cannot be tuned for the given recognition task. The latent pose estimator encodes the knowledge of multimodal image-to-pose relationship and provides optimal feature representation for action recognition. This knowledge can be acquired from existing well-trained models (if available) and adapted for action recognition in the learning process. In all, the latent pose estimator is seamlessly integrated and globally optimized with the random fields.

The model parameters $\Omega = \{\Phi, \Theta\}$ are learned from training data consisting of labeled action sequences $(X^{(t)}, \mathbf{z}^{(t)})$. The labeled image-to-pose data $(\mathbf{x}^{(t)}, \mathbf{y}^{(t)})$, if available, can also be utilized as auxiliary data. The optimal parameters Ω^* is obtained by maximizing the objective function:

$$L(\Omega) = \underbrace{\sum_t \log P(\mathbf{z}^{(t)}|X^{(t)}, \Omega)}_{L_1(\Omega)} \underbrace{-\frac{1}{2\sigma^2}\|\Phi\|^2}_{L_2(\Omega)} + \eta \underbrace{\sum_t \log P(\mathbf{y}^{(t)}|\mathbf{x}^{(t)}, \Theta)}_{L_3(\Omega)} \tag{8}$$

where the first term, denoted as $L_1(\Omega)$, is the conditional log-likelihood of the action training data. The second term $L_2(\Omega)$ is the log of Gaussian prior $P(\Phi) \sim \exp\left(-\frac{1}{2\sigma^2}\|\Phi\|^2\right)$ with variance σ^2 and it prevents Φ from drifting too much. And the third term $L_3(\Omega)$ is the conditional log-likelihood of the image-to-pose training data. η is a constant learning rate. Note that our model enables the image-to-pose data to be naturally added to the learning process.

3.2 The Latent Pose Estimator

The image-to-pose relation is highly non-linear. Fortunately, close observation of human images shows that human appearance changes very fast as the human global orientation changes, while the appearance changes relatively slowly in a fixed orientation. Therefore, we may assume that the image-to-pose distribution in a fixed orientation can be well modelled by a single or a combination of linear regressor(s). This leads us to use the Bayesian mixtures of experts (BME) [16] to model the multi-modal image-to-pose distributions. Suppose $\mathbf{x}$ is the visual feature of the image and $\mathbf{y}$ is the human pose, the model with M experts is:

$$p(\mathbf{y}|\mathbf{x}, \Theta) = \sum_{i=1}^{M} g(\mathbf{x}, \nu_i) p(\mathbf{y}|\mathbf{x}, T_i, \Lambda_i) \tag{9}$$

where

$$g(\mathbf{x}, \nu_i) = \frac{e^{\nu_i^T \mathbf{x}}}{\sum_j e^{\nu_j^T \mathbf{x}}} \tag{10}$$

$$p(\mathbf{y}|\mathbf{x}, T_i, \Lambda_i) \sim \mathcal{N}(\mathbf{y}; T_i \mathbf{x}, \Lambda_i) \tag{11}$$

Here $\Theta = \{\nu_i, T_i, \Lambda_i | i = 1, 2, \cdots, M\}$ consists of the parameters of the BME model. The *expert* $p(\mathbf{y}|\mathbf{x}, T_i, \Lambda_i)$ is an Gaussian distribution with mean $T_i\mathbf{x}$ and covariance matrix Λ_i. The mixing proportions of the experts, $g(\mathbf{x}, \nu_i)$, are *input dependent* and work like gates that can competitively switch-on multiple experts for some input domains, allowing multi-modal conditionals. They can also pick a single expert for unambiguous inputs by switching-off other experts. Given the input $\mathbf{x}$ and parameters Θ, the optimal pose estimation of the BME model is

$$\mathbf{y}^* = \int \mathbf{y} P(\mathbf{y}|\mathbf{x}, \Theta) d\mathbf{y} = \sum_{i=1}^{M} g(\mathbf{x}, \nu_i) T_i \mathbf{x} \tag{12}$$

The BME model has exhibited success in representing image-to-pose distributions in the literature [6]. But our LPCRF model is not limited to the BME representation. We can replace the BME model with any other differentiable discriminative models without major modifications to our LPCRF structure.

3.3 Learning Model Parameters

We use an iterative gradient ascent algorithm to search for the optimal model parameters that maximize the objective function, *i.e.*, $\Omega^* = \arg\max_\Omega L(\Omega)$. At each iteration, Ω can be updated by $\Omega \leftarrow \Omega + \xi \frac{\partial L(\Omega)}{\partial \Omega}$ or any other Quasi-Newton methods, where ξ is the learning rate. First, we compute $\partial L(\Omega)/\partial \Phi$ for estimation of Φ.

$\partial L(\Omega)/\partial \Phi$ can be obtained by summarizing the gradients of $\log P(\mathbf{z}|X,\Omega)$ with respect to Φ over all training samples (X, z). According to the chain rule, the gradient $\partial \log P(\mathbf{z}|X,\Omega)/\partial\phi$ for a parameter $\phi \in \Phi$ is

$$\frac{\partial \log P(\mathbf{z}|X,\Omega)}{\partial \phi} = \sum_{j,a} \frac{\partial \log P(\mathbf{z}|X,\Omega)}{\partial V_{ja}} \frac{\partial V_{ja}}{\partial \phi} + \sum_{j,a,b} \frac{\partial \log P(\mathbf{z}|X,\Omega)}{\partial E_{jab}} \frac{\partial E_{jab}}{\partial \phi} \tag{13}$$

Given Eqn. 4 and 5, the gradients $\partial V_{ja}/\partial\phi$ and $\partial E_{jab}/\partial\phi$ are the corresponding feature function. And the gradients $\partial \log P(\mathbf{z}|X,\Omega)/\partial V_{ja}$ and $\partial \log P(\mathbf{z}|X,\Omega)/\partial E_{jab}$ can be expressed in terms of the marginal probabilities over individual vertex j or edge $(j-1, j)$,

$$\frac{\partial \log P(\mathbf{z}|X,\Omega)}{\partial V_{ja}} = P(h_j = a|\mathbf{z}, Y, \Phi) - P(h_j = a|Y, \Phi) \tag{14}$$

$$\frac{\partial \log P(\mathbf{z}|X,\Omega)}{\partial E_{jab}} = P(h_{j-1} = a, h_j = b|\mathbf{z}, Y, \Phi) - P(h_{j-1} = a, h_j = b|Y, \Phi) \tag{15}$$

These marginal probabilities can be efficiently calculated using belief propagation [3] due to the chain structure of the random fields.

Learning the parameters Θ involves computation of $\partial L_1(\Omega)/\partial\Theta$ and, if image-to-pose training data are available, $\partial L_3(\Omega)/\partial\Theta$. The gradient $\partial L_3/\partial\Theta$ is the sum of the gradients of the BME model that can be found in [16]. To obtain $\partial L_1(\Omega)/\partial\Theta$, we rely on the chain rule to compute

$$\frac{\partial \log P(\mathbf{z}|X,\Omega)}{\partial \Theta} = \sum_{j,a} \frac{\partial \log P(\mathbf{z}|X,\Omega)}{\partial V_{ja}} \frac{\partial V_{ja}}{\partial \mathrm{vec}(Y)} \frac{\partial \mathrm{vec}(Y)}{\partial \Theta} \tag{16}$$

for specific training sample (X, z). Here, $\mathrm{vec}(A)$ is the stacked columns of A, and Y is the optimal estimation of the latent pose estimator (by Eqn. 12) given X and current estimation Θ. In Eqn. 16, we assume the transition functions t_k are independent of Y. The gradient $\partial V_{ja}/\partial\mathrm{vec}(Y)$ depends on the definition of state functions. Note that the chain rule decouples the gradient $\partial \log P(\mathbf{z}|X,\Omega)/\partial\Theta$ into three simple factors. The value of the factor $\partial \log P(\mathbf{z}|X,\Omega)/\partial V_{ja}$ has already been computed by Eqn. 14 in estimation of Φ and is back propagated to the latent pose layer for estimation of Θ. The feature functions are entirely isolated into a single factor $\partial V_{ja}/\partial \mathrm{vec}(Y)$. And the third factor consists of all the calculations on the latent pose estimator. Thus, the decoupling allows flexible deployment of feature functions and latent pose estimator without increasing the complexity of gradient computations.

Computation of the product of $\partial V_{ja}/\partial \mathrm{vec}(Y)$ and $\partial \mathrm{vec}(Y)/\partial\Theta$ is straightforward. Note that $L_1(\Omega)$ does not explicitly depend on the covariance matrixes of the BME model, *i.e.*, Λ_i cannot be updated from action data. We use image-to-pose data (if available) to update Λ_i, or directly use the Λ_i of an existing well-trained BME model, or, if both are not available, just assume constant covariance matrixes.

3.4 Feature Functions

In our model, the feature functions are differentiable with respect to the latent poses so that gradient ascent algorithm are applicable. Our feature functions resemble the well-known *logit model* and are widely used in the literature [4,3]. We have $|\mathcal{H}|\times|\mathcal{H}|$ transition functions and each corresponds to a hidden variable pair (h, h'), denoted by $t_{hh'}$:

$$t_{hh'}(j, h_{j-1}, h_j, Y) = \delta(h, h_{j-1})\delta(h', h_j). \tag{17}$$

The corresponding parameters $\mu_{hh'}$ form an $|\mathcal{H}| \times |\mathcal{H}|$ matrix that is essentially a transition matrix. It models both the external dynamics between actions and the internal substructures of individual actions [4].

To make the computation tractable, the state functions do not model the dependency of the entire observation sequence but, instead, depend only on a window around the current frame. In other words, $s_k(j, h_j, Y) = s_k(j, h_j, \tilde{Y}_j)$, where $\tilde{Y}_j = [\mathbf{y}_{j-w}, \cdots, \mathbf{y}_{j+w}]$ is a window around the j-th frame with window size $2w+1$. Assume $\mathbf{y}_j$ has dimension d. We have $|\mathcal{H}|\times d(2w+1)$ state functions, and each corresponds to a pair (h, l), where $1 \le l \le d(2w+1)$. The state function $s_{hl}(j, h_j, Y) = \delta(h, h_j)\tilde{Y}_j(l)$, where $\tilde{Y}_j(l)$ is the l-th entry in $\tilde{Y}_j$. With the window feature, $\partial V_{ja}/\partial Y$ is a sparse matrix $\left[\mathbf{0}^{d\times(j-w-1)}, \tilde{\lambda}_a, \mathbf{0}^{d\times(n-j-w)}\right]$, where $\tilde{\lambda}_a$ is a $d \times (2w + 1)$ matrix consisting of the parameters λ_{al} corresponding to all s_{al} for a fixed $a \in \mathcal{H}$. Thus, Eqn. 16 can be further simplified.

3.5 Inference

Given the model parameters Ω^* learned from the training data, prediction of a new test sequence X is to estimate the most probable sequence labels $\mathbf{z}^*$ that maximizes our model

$$\mathbf{z}^* = \arg\max_{\mathbf{z}} P(\mathbf{z}|X, \Omega^*) = \arg\max_{\mathbf{z}} P(\mathbf{z}|Y^*, \Phi^*) \tag{18}$$

where Y^* is the optimal pose estimation given X and Θ^*.

The sequence labels $\mathbf{z}^*$ can be estimated using either Viterbi path [3] or marginal probabilities [4]. We choose the later for this paper. We compute for each frame i the marginal probabilities $P(h_i = a|Y^*, \Phi^*)$ for all $a \in \mathcal{H}$. The marginal probabilities are summed according to the sets of hidden states $\mathcal{H}_z$. The label z_i^* associated with the set having maximum summed marginal probabilities is assigned to frame i. As we mentioned in Section 3.3, $P(h_i = a|Y^*, \Phi^*)$ can be efficiently computed using belief propagation. Thus, the inference operation is also very efficient.

4 Experimental Results

HumanEva dataset. We test the effectiveness of our approach on a real human motion dataset–HumanEva–made publicly available by the Brown Group [1]. The dataset was captured simultaneously using a calibrated marker-based motion capture system and multiple high-speed video capture systems. It contains multiple subjects performing a set of predefined actions with repetitions, and was originally partitioned into *Train*, *Validate*, and *Test* sub-sets. Fig. 4(a) (top) gives a sample image. We choose 4 actions[1]: *Walking*, *Box*, *Jog*, and *Gestures*, performed by subjects S1, S2 and S3, captured by cameras C1, C2, and C3. There are 56,261 video frames in total. Note that our model will recognize actions under different view points.

The original motion data provided by HumanEva were (x, y, z) locations of the body parts in the world coordinate system. There is a total of 10 parts: torso, head, upper and lower arms, and upper and lower legs. In this work, we discard the internal parameters of the human body model (like limb length), and convert the (x, y, z) locations to global orientation of torso and relative orientation of adjacent body parts. Each orientation is represented by 3 Euler angles.

Visual features for image representation. We choose the bag-of-words model [17] to represent the human images, because it is resistant to a large misalignment of the human region in the detection window that may pose difficulties to many other representations. For each video frame, the human window is detected by human detector or background subtraction and is scaled to a fixed size. In the human window, we extract a set of local descriptors, called *Appearance and Position Context (APC) descriptor* [18]. The bag-of-words representation of this frame is a 300-bin histogram of the APC descriptors.

Comparison of different models. We run several experiments in order to compare CRF and LDCRF with our LPCRF model under different configurations. The training data include all videos in both *Train* and *Validate* subsets with 25,645 frames, and the testing data include the videos in the *Test* subset with 30,616 frames. The window size w for the feature function is set to 3, *i.e.*, the context of observations of 7 frames is explored at current positions. All models have 4 states, each corresponding to an action class. The number of hidden

[1] The *ThrowCatch* action is not selected, because we failed to extract video frames from S1_Validate and S3_Train/Validate, and have frequent frame drops in S1_Train and S2_Train/Validate, even using the tool provided by the HumanEva dataset itself.

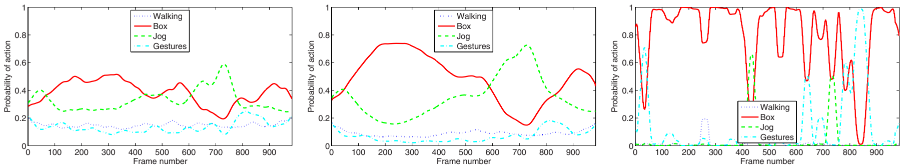

(a) CRF (b) LDCRF (c) $LPCRF_{pure}$

Fig. 2. Probability of actions on sequence S2_Box_Test_C3. Both CRF (a) and LDCRF (b) have much uncertainty in labeling this sequence, achieving recognition rate of 69.5% and 70.5%, respectively. Our $LPCRF_{pure}$ model (c) significantly improves the recognition rate to 85.6%, even without using pose knowledge. Best viewed in color.

states for each action class is chosen as 3 for both LPCRF and LDCRF. We use 5 experts for the BME model. In testing, each video frame is labelled as one of the 4 actions that has maximum marginal probabilities. Here, the recognition rate is computed based on frames, not on sequences, because each sequence is very long and this metric is also appropriate for unsegmented sequences.

Our LPCRF model is tested under 4 configurations. 1) $LPCRF_{init}$: the parameters Θ of the latent pose estimator are initialized using the parameters of an existing BME model that is well-trained on 5,000 frames randomly selected from the *Train* subset, and then are further updated iteratively on action videos. 2) $LPCRF_{fix}$: Θ are initialized using the same BME model but are fixed in the learning process. Essentially, it is an LDCRF trained on pose sequences that are obtained by an existing BME model. 3) $LPCRF_{xy}$: the model is randomly initialized, but uses training data including both action videos and 1,000 extra image-to-pose pairs selected from the *Train* subset. 4) $LPCRF_{pure}$: it is also randomly initialized but trained purely on action data, *i.e.*, it does not utilize image-to-pose knowledge and data, and uses a setup as CRF and LDCRF.

In Table 1, Figs. 2, **??**, and 3, we analyze the the performance of the six models. Table 1 gives the confusion matrixes and average recognition rates of these models. From them, we note that: 1) The $LPCRF_{pure}$ outperforms CRF and LDCRF without using any pose-to-image data. This demonstrates the effectiveness using a trainable feature extractor to compress the high dimensional observations into more informative and compact feature vectors. This trainable feature extractor decreases the complexity of the random fields, and, in turn, increases the performance. 2) With additional image-to-pose data, $LPCRF_{init}$ and $LPCRF_{xy}$ achieve the best performance, which demonstrates that our model effectively transfers the knowledge on image-to-pose relationship to the new vision task of action recognition. 3) $LPCRF_{fix}$ is essentially a LDCRF but it outperforms the latter. It concludes that the estimated human poses, compared with the original visual features, are more powerful in action recognition. 4) $LPCRF_{init}$ achieves a higher performance than $LPCRF_{fix}$, although both are initialized by the same BME model. This means that further updating of the

Table 1. Confusion matrixes of six models. The last row of each table gives model name and the average recognition rate. $LPCRF_{init}$ achieves the best performance 95.0%.

	wlk	*box*	*jog*	*gest*
wlk	**95.0**	0.1	4.9	0
box	0.4	**79.4**	10.9	9.3
jog	4.3	3.9	**89.7**	2.1
gest	1.6	25.0	0	**73.4**
	CRF: 85.0			

wlk	*box*	*jog*	*gest*
96.3	0	3.7	0
0	**75.0**	16.2	8.8
0	1.4	**97.3**	1.3
0.2	21.4	0	**77.4**
LDCRF: 87.2			

wlk	*box*	*jog*	*gest*	
97.8	0	0.2	2.0	*wlk*
0.9	**92.5**	5.8	0.8	*box*
0.4	0.2	**99.4**	0	*jog*
2.4	7.9	0.1	**89.6**	*gest*
$LPCRF_{init}$: **95.0**				

	wlk	*box*	*jog*	*gest*
wlk	**94.8**	0	0.5	4.7
box	1.0	**89.2**	8.6	1.2
jog	0.2	0.4	**99.4**	0
gest	2.9	11.8	0.3	**85.1**
	$LPCRF_{fix}$: 92.3			

wlk	*box*	*jog*	*gest*
95.6	0	0.7	3.7
0.8	**89.5**	6.5	3.2
0.5	0	**99.4**	0.1
0	10.9	0.6	**88.5**
$LPCRF_{xy}$: 93.4			

wlk	*box*	*jog*	*gest*	
95.5	0.4	2.2	1.9	*wlk*
2.2	**79.5**	7.6	10.7	*box*
4.5	0.9	**94.6**	0	*jog*
5.5	11.3	0.4	**82.8**	*gest*
$LPCRF_{pure}$: 88.5				

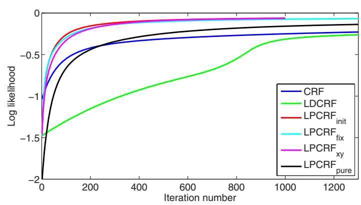

(a) Log likelihood

model	CRF	LDCRF	$LPCRF_{init}$	$LPCRF_{fix}$	$LPCRF_{xy}$	$LPCRF_{pure}$
Train Time(s)	2.5	3.2	22.1	2.8	22.3	22.1
Test Time(s)	1.62	2.14	2.08	2.08	2.08	2.08

(b) Run time

Fig. 3. (a) Log likelihood versus the iteration number for the six models. Note that $LPCRF_{init}$, $LPCRF_{fix}$, and $LPCRF_{xy}$ converge in about 400 iterations, and CRF, LDCRF, and $LPCRF_{pure}$ in about 1000 iterations. (b) Training time for one iteration and testing time for labeling the entire testing set. Best viewed in color.

latent pose estimator using action data does improve the performance, even after it is well-initialized. 5) Finally, LDCRF outperforms CRF on this dataset, which is also consistent with the conclusion in [4]. Fig. 2 shows the probability of actions on sequence S2_Box_Test_C3 assigned by models CRF, LDCRF, and $LPCRF_{pure}$. CRF and LDCRF have much uncertainty in labeling this sequence, and the uncertainty is largely reduced by our $LPCRF_{pure}$ model.

Fig. 3(a) gives the log-likelihood versus the iteration number for the six models. $LPCRF_{init}$, $LPCRF_{fix}$, and $LPCRF_{xy}$ converge quickly in about 400 iterations with auxiliary knowledge or data on human pose, compared to 1,000 iterations required by the other three that are randomly initialized. On the other hand, our LPCRF model (except $LPCRF_{fix}$) requires training time for each iteration as much as 8 times of that by CRF and LDCRF (see Fig. 3(b)). Most of the extra time is used for updating the parameters of latent pose estimator.

Table 2. Testing of upper bound performance. The performance of LDCRF (**Left**) trained on the ground truth human poses is supposed to be the upper bound of our LPCRF model (**Right**) trained on video data. Both models are trained on the corresponding *Train* subset and tested on the *Validate* subset. The last row gives the average recognition rate. *wlk*: Walking, *gest*: Gestures.

	wlk	*box*	*jog*	*gest*
wlk	**100**	0	0	0
box	0	**98.5**	0	1.5
jog	0	0	**100**	0
gest	19.5	1.4	0	**79.1**
LDCRF: 95.2%				

wlk	*box*	*jog*	*gest*	
99.6	0	0.2	0.2	*wlk*
0	**98.9**	0	1.1	*box*
0	1.0	**99.0**	0	*jog*
27.4	2.1	6.8	**63.7**	*gest*
$LPCRF_{init}$: 91.7%				

But our model achieves testing speed as fast as LDCRF and slightly slower than CRF. It takes about 2.1 seconds to label the entire testing set. Note that the time given in Fig. 3(b) does not include the time for feature extraction. And our program is pure MATLAB code and run on a laptop with 2GHz dual core CPU.

Upper bound performance. The performance of a conditional random fields model trained directly on the ground truth human poses is expected to be the upper bound of our model trained on video sequences. This is because the regression error of the latent pose estimator might degrade the performance, and our model reaches the upper bound if the latent pose estimator works perfectly. To demonstrate how much our model can achieve, we train an LDCRF on the ground truth human poses in the *Train* subset and test it on the *Validate* subset (note that the ground truth is unavailable in the *Test* subset), and train and test an $LPCRF_{init}$ model on the same subsets but using video data. Table 2 shows the performance in confusion matrix format. Our $LPCRF_{init}$ model trained on video achieves a recognition rate 91.7% that is close to the upper bound 95.2% given by LDCRF that is trained on ground truth human poses. Note that these rates are not comparable with those in Table 1 because here we use a different setup of training and testing sets.

Label unsegmented videos. It is natural to apply conditional random fields models to label unsegmented video sequences. Because there are no individual sequences in HumanEva consisting of all studied actions, we manually generate a new sequence by concatenating four action clips chosen from S1_Test_C1. Inference is done on the entire sequence. Our LPCRF models achieve a recognition rate higher than 97%, while the rates are 74.2% and 75.2% for CRF and LDCRF, respectively. See details in the first part of Table 3.

To further verify the generalization ability of our model, we apply the six models that are trained on HumanEva (setup is as above) to label some free-style action videos. These videos are unsegmented with resolution 640×480. And the scenes and subjects are completely different from that in HumanEva. Fig. 4(a) gives two sample images, selected from the HumanEva (top) and free style videos (bottom), respectively. In each free style video, a subject performs the four

Table 3. Accuracy of labeling unsegmented video sequences. The models are trained on the *Train* and *Validate* subsets of HumanEva. **First part**: a manually concatenated sequence with four action clips. **Second part**: two free-style videos with scenes and subjects completely different from HumanEva. See video illustrations in the supplemental materials.

seq	frm #	CRF	LDCRF	$LPCRF_{init}$	$LPCRF_{fix}$	$LPCRF_{xy}$	$LPCRF_{pure}$
S1_Test_C1	1207	74.2	75.2	**99.8**	99.0	99.5	97.2
Free style 1	910	71.4	64.8	80.1	80.9	**86.4**	81.7
Free style 2	1060	33.7	34.0	**76.4**	75.3	64.9	72.8

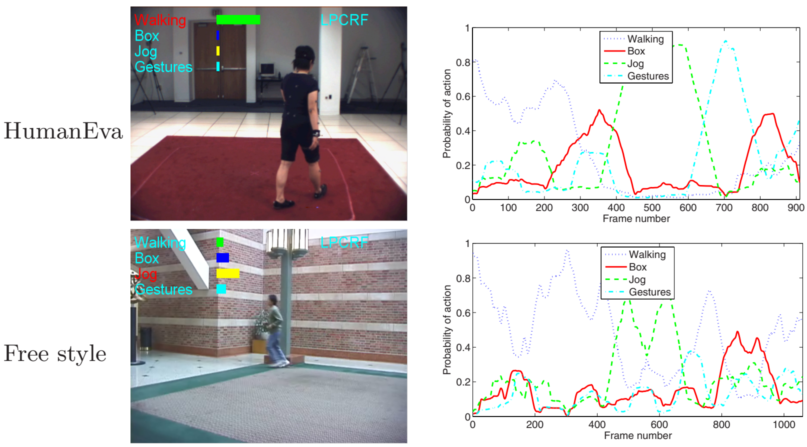

(a) Sample images (b) Probability of actions

Fig. 4. (a) Two sample images selected from HumanEva (**top**) and free-style videos (**bottom**), respectively. Colored bars indicate action probabilities. (b) Probability of actions on free-style sequence 1 (**top**) assigned by $LPCRF_{xy}$ and on free-style sequence 2 (**bottom**) assigned by $LPCRF_{init}$. See better illustration in supplemental videos.

actions in arbitrary order, with arbitrary number of repetitions, and from arbitrary view angles. Challenges of these videos include: 1) varying view angle of actions; 2) varying scale of subjects; 3) a plant and pillar in the background having color very close to the clothes; and 4) rich textures on the wall.

The second part of Table 3 gives the labeling accuracy by the six models. The corresponding action probability of these two free-style sequences is shown in Fig. 4(b). Again, our LPCRF models achieve a significant improvement over CRF and LDCRF. Especially, $LPCRF_{init}$ produces very promising results. This shows that image-to-pose knowledge obtained from one dataset could be utilized to label video sequences outside of this dataset. We use the background subtraction code provided by HumanEva dataset to locate the human in these two sequences. It does not work reliably under this more challenging environment. Nonetheless, our models trained on HumanEva dataset still achieve reasonable performance on these videos. We expect that a more accurate human detector will largely improve the performance.

Discussions. Our model achieves best performance when the human is close to camera and image-to-pose knowledge is available. Thus, it is more appropriate to recognize subtle actions and be applied in HCI. We did not verify it on videos where the subjects are tiny and/or blurred (*e.g.*, surveillance videos). In this paper, our model is applied to human action recognition, but it can be easily generalized to other applications such as sign language translation, or in a more general form, used for application-specific feature compression.

5 Conclusion

We proposed a novel model to bridge the gap between the high dimensional observations and the random fields. This model replaces the observation layer of random fields with a latent pose estimator that learns to convert the high dimensional observations into more compact and informative representations under the supervision of labeled action data. The structure of our model also enables transfer learning to utilize the existing knowledge and data on image-to-pose relationship. Our model is tested on a real human motion dataset, and achieves significant improvement over the standard CRF and its variations.

References

1. Sigal, L., Black, M.J.: Humaneva: Synchronized video and motion capture dataset for evaluation of articulated human motion. Tech. Report, Brown Univ. (2006)
2. Rabiner, L.R.: A tutorial on hidden markov models and selected applications in speech recognition. Proceedings of the IEEE 77(2), 257–286 (1989)
3. Lafferty, J.D., Mccallum, A., Pereira, F.C.N.: Conditional random fields: Probabilistic models for segmenting and labeling sequence data. In: ICML, pp. 282–289 (2001)
4. Morency, L.P., Quattoni, A., Darrell, T.: Latent-dynamic discriminative models for continuous gesture recognition. CVPR (2007)
5. Sminchisescu, C., Kanaujia, A., Metaxas, D.: Conditional models for contextual human motion recognition. Comput. Vis. Image Underst. 104(2), 210–220 (2006)
6. Sminchisescu, C., Kanaujia, A., Metaxas, D.: Bm^{3}e: Discriminative density propagation for visual tracking. PAMI (2007)
7. Agarwal, A., Triggs, B.: Recovering 3d human pose from monocular images. IEEE Transactions on Pattern Analysis and Machine Intelligence (2006)
8. Caruana, R.: Multitask learning. Machine Learning 28(1), 41–75 (1997)
9. Lv, F., Nevatia, R.: Single view human action recognition using key pose matching and viterbi path searching. CVPR (2007)
10. Blank, M., Gorelick, L., Shechtman, E., Irani, M., Basri, R.: Actions as space-time shapes. In: ICCV, pp. 1395–1402 (2005)
11. Ramanan, D., Forsyth, D.A.: Automatic annotation of everyday movements. In: NIPS (2004)
12. Cuntoor, N.P., Chellappa, R.: Epitomic representation of human activities. CVPR (2007)

13. Yilmaz, A., Shah, M.: Recognizing human actions in videos acquired by uncalibrated moving cameras. In: ICCV (2005)
14. Quattoni, A., Collins, M., Darrell, T.: Conditional random fields for object recognition. Neural Information Processing Systems (2004)
15. Hammersley, J.M., Clifford, P.: Markov field on finite graphs and lattices (unpublished manuscript, 1971)
16. Jordan, M., Jacobs, R.: Hierarchical mixtures of experts and the em algorithm. Neural Computation 6, 181–214 (1994)
17. Fei-Fei, L., Perona, P.: A bayesian heirarchical model for learning natural scene categories. In: Proc. CVPR (2005)
18. Ning, H., Xu, W., Gong, Y., Huang, T.: Discriminative learning of visual words for 3d human pose estimation. CVPR (2008)